Supplemental Data

Extent of intravital contraction of arterial and venous thrombi and pulmonary emboli

Rafael R. Khismatullin[1,2], Shahnoza Abdullayeva[2], Alina D. Peshkova[2],

Khetam Sounbuli[2], Natalia G. Evtugina[2], Rustem I. Litvinov[1,2], John W. Weisel[1]

[1]Department of Cell and Developmental Biology, University of Pennsylvania School of Medicine, Philadelphia, Pennsylvania, USA

[2]Institute of Fundamental Medicine and Biology, Kazan Federal University, Kazan, Russian Federation

Supplemental Materials and Methods

In vitro blood clots with various extents of contraction from normal blood

Human blood samples were collected from healthy donors according to a protocol approved by the Ethical Committee of the Interregional Clinical Diagnostic Center, Kazan, Russian Federation (Reference #70 as of 30.01.2016) and in compliance with the Declaration of Helsinki. Written informed consent was obtained from each donor. Venous blood was stabilized with 3.8% trisodium citrate 9:1 by volume and used within 4 hours after withdrawal. To form a blood clot and induce clot contraction, 1.2 ml of citrated blood in a conical Eppendorf 1.5-ml tube was activated by the addition of 2 mM $CaCl_2$ and 1 U/ml human thrombin (final concentrations). The clots formed within ½ minute and were allowed to contract at 37°C for various periods of time up to 60 minutes. The tubes were pre-lubricated with 4%v/v Triton X-100 in saline to prevent the attachment of fibrin to the walls and allow unconstrained clot shrinkage. At various time points, the clot contraction was stopped by immersing the clots into 10× excessive volume of a fixative: either formalin (for histology) or glutaraldehyde (for scanning electron microscopy). The extents of volumetric shrinkage were determined from photographic images of the fixed clots (Figure S2). 36 *in vitro* clots made from the blood of 9 independent donors were analyzed (2 clots from each donor fixed at each time point in duplicate, one for histology and one for scanning electron microscopy). The composition of the blood used in the measurements has been reported, namely hematocrit, platelet counts and fibrinogen levels (Table S7).

In vitro blood clots with various extents of contraction from pathological blood

Human blood samples were collected from 23 patients with acute COVID-19 who were hospitalized in the City Hospital No. 16, Kazan, Russian Federation and subjected to scanning electron microscopy (SEM). The study was approved by the Ethics Committee of the Kazan (Volga region) Federal University (Resolution # 27 as of December 28, 2020. In accordance with the guidelines issued by the Ministry of Public Health of the Russian Federation, all the patients enrolled in this study received standard treatment, including immunosuppressive medications and low molecular weight heparin. Written informed consent was obtained from each donor. Clinical characteristics of the patients enrolled in the study and their blood composition are summarized in Tables S2 and S3.

Venous blood was stabilized with 3.8% trisodium citrate 9:1 by volume and used within 4 hours after withdrawal. To form a blood clot and induce clot contraction, 1.2 ml of citrated blood in a conical Eppendorf 1.5-ml tube was activated by the addition of 2 mM $CaCl_2$ and 1 U/ml human thrombin (final concentrations). The blood samples were clotted and allowed to fully contract followed by fixation and processing of the contracted clots for SEM as described above for the clots from normal blood. The tubes were pre-lubricated with 4%v/v Triton X-100 in saline to prevent the attachment of fibrin to the walls and allow unconstrained clot shrinkage. *In vitro* clots made from the blood of 23 patients were analyzed (at least 5 images for each clot) using SEM.

Venous thrombi and pulmonary emboli

Mechanical extraction of 13 deep vein thrombi was performed at the Interregional Clinical Diagnostic Center (ICDC, Kazan, Russian Federation). The study was approved by the Ethical Committee of ICDC (protocol No. 70 as of January 30, 2016). The venous thrombi were obtained in accordance with the approved guidelines, including informed written consent obtained from the patients. 6 pulmonary thrombotic emboli from autopsies performed on patients who died of pulmonary embolism were obtained from the Department of Pathology and Laboratory Medicine at the Hospital of the University of Pennsylvania. The

venous thrombi and pulmonary emboli were obtained from patients receiving standard antithrombotic treatment with no significant differences in the gender and age. Immediately after extraction, all the samples were placed into the fixative (2% glutaraldehyde) and later processed for scanning electron microscopy. The venous thrombi were cut into three parts, namely the head, body, and tail; the head was attached to the vessel wall and comprised the oldest portion of the thrombus, while the tail (usually freely mobile in the vessel lumen) was the youngest. The overall demographic and clinical characteristics of patients with deep venous thrombosis and pulmonary embolism enrolled in this study are presented in Tables S8 and S9.

Cerebral arterial thrombi

Mechanical thrombectomy of 24 cerebral arterial thrombi was performed in the University Hospital Ostrava, Interventional Neuroradiology and Angiology Department, Czech Republic. The design of this study was approved by the local ethical committee (Reference: 639/2017). All patients provided written informed consent to participate in the study. All patients included in the study had confirmed large vessel thromboembolic occlusion. The 24 thrombi extracted using mechanical thrombectomy were immediately placed into a transport vial containing fixative and further processed for scanning electron microscopy. The overall demographic and clinical characteristics of patients with acute ischemic stroke involved in this study are presented in Table S10.

Histology

For histological examination, *in vitro* blood clots with varying extents of contraction were fixed in 10% neutral buffered formalin for at least 24 hours, washed in water, treated consequently with ascending concentrations of isopropanol and xylene using a tissue processor (STP420ES, Thermo Fisher Scientific), and embedded in paraffin. Each blood clot was cut longitudinally, sliced into four-micrometer-thick sections that were stained with hematoxylin and eosin (H&E) or Picro-Mallory stains. The slides were analyzed in a Zeiss Axio Imager Z2 microscope at 400x magnification, which allowed discerning the spatial distribution of clot components (Figures 2 and S4). A total of 180 microscope slides were analyzed (stained with 2 techniques) from 18 clots with 5 various extents of contraction obtained from 9 independent blood samples. It is noteworthy that each blood clot, which reproduced the shape of a 1.5-ml Eppendorf tube, was cut longitudinally through the middle, visualized in a microscope, and its parts were measured as shown in Figure S5.

Scanning electron microscopy (SEM)

In vitro blood clots and *ex vivo* thrombi were fixed in 2% glutaraldehyde in phosphate-buffered saline, pH 7.4, for at least 24 hours. Following fixation, each blood clot or thrombus was cut-open longitudinally so that both the interior part and the edges could be viewed. The fixed samples were rinsed in 50 mM cacodylate buffer, pH 7.4, containing 150 mM sodium chloride, then dehydrated in ethanol at increasing concentrations of 30-100 vol%, dried with hexamethyldisilazane, and sputter-coated with gold-palladium (Polaron e5100, Quorum Technologies, UK). High-resolution micrographs of *in vitro* blood clots were taken from the outer layer as well as from intermediate and central parts (Figures 4A and S6). To eliminate selection bias, images of *ex vivo* thrombi were obtained from randomly chosen areas of each sample. Micrographs were obtained using an FEI Quanta 250FEG scanning electron microscope (FEI, Hillsboro, OR).

Using scanning electron micrographs to quantify the composition of blood clots and thrombi

In the scanning electron micrographs of contracted blood clots and thrombi, the following structural elements were identified (Figure 1A): biconcave RBCs (discoid shape with a clear dimple in the middle) (Figure 1A1), intermediate mainly biconcave RBCs (no longer typical biconcave but round and smooth with no visible edges and no pronounced or faint dimple in the middle) (Figure 1A2), intermediate mainly polyhedral RBCs (the surface formed of mostly flat sides with visible edges except some rounded or wavy edges) (Figure 1A3), polyhedral RBCs or polyhedrocytes (the surface made up of polygons with pronounced edges, tightly packed) (Figure 1A4), and fibrin appearing as filamentous (Figure 1A5) or spongy (Figure 1A6) structures. The composition of blood clots and thrombi was quantified using Image J 1.48 software (National Institutes of Health, Bethesda, MD, USA). In particular, a scanning electron micrograph was transposed onto a computer screen, a fine grid was overlaid onto the image, and each square of the grid was marked for the element(s) that it contained. Grid squares 14 μm x 14 μm were applied for blood clot images taken at a 500× magnification (Figure 1B) and 6 μm x 6 μm grid squares were applied for images of thrombi obtained at a 2,000× magnification (Figure S1). RBCs were quantified as the number of each cell type per image. RBCs located at the square edges were assigned to the grid square that contained a greater portion of the cell. Therefore, each cell was counted only once. For fibrin, we measured the rough percentage of each grid square occupied by fibrin and the total fibrin area in each image. A grid facilitates visual image analysis, but it is not essential for calculation of the number of each cell type; it is needed for quantification of the area occupied by non-cellular structures (spaces and fibrin). The sizes of grid squares depended on the image magnification and the area covered, but did not affect results on cellular composition of contracted clots. Below we provide two images of the same clot at 2,000× and 500× normalized by the area covered along with the polyhedral/biconcave RBC ratios obtained for each image (Figure S12). At 500× magnification, more cells can be analyzed at a time, but the results from the same area of a thrombus were independent of the magnification and grid size. To reduce the human error, qualitative conclusions were established by examination of all images by 3 independent observers who were blinded to the source of the material except the lead organizer. Internal reproducibility was established by re-quantifying a representative set of images from some of the same specimens by different examiners. After observers were trained, inter-observer variation was negligible. Patterns in the structure and composition were visually apparent by observations of hundreds of images. The process of image quantification takes several hours per image.

A total of 135 SEM images of the outer, intermediate, and central areas of in vitro blood clots were obtained and analyzed from 15 clots from normal blood samples with various extents of contraction. A total of 115 images of randomly selected areas were obtained and analyzed from 23 contracted clots formed from pathological blood samples of COVID-19 patients. A total of 117 images of randomly selected areas were obtained from the head, body, and tail of 13 venous thrombi. A total of 18 images of randomly selected areas were obtained and analyzed from 6 pulmonary thrombotic emboli. A total of 120 images of randomly selected areas were obtained and analyzed from 24 cerebral arterial thrombi.

Statistical analysis

Statistical analysis was performed using the GraphPad Prism 7 software package. Normality of data distribution was determined by the D'Agostino-Pearson, Shapiro-Wilk and Kolmogorov-Smirnov criteria. Multi-group analyses were performed by the one-way ANOVA (parametric) test for normal distribution; for data with non-normal distribution, the nonparametric Friedman test with post hoc Benjamini, Krieger and Yekutieli tests or the Kruskal–Wallis test (when the type of distribution in the compared groups was the same) with Dunn's post hoc test were performed. For pairwise comparisons, the Mann-Whitney test

(nonparametric) was performed. The categorical values (yes/no) were analyzed using the chi-square test. A significance level of 0.05 was applied in all types of statistical analysis.

Supplemental Results

Section S1. *Details of microscopically revealed spatial segregation of in vitro blood clots during the time course of contraction*

The dense inner portion and relatively loose outer layer of a clot in the microscope slides are clearly discernible at the higher extents of clot contraction (~50% and ~60%), while at the lower degrees of clot shrinkage (~20% and ~30%) the boundaries between the outer layer and more tightly packed inner portion are not very distinct (Figures 2 and S4). A relatively narrow transition zone was often observed at the higher extents of contraction (50% and 60%) with a gradient from a denser to a looser cell packing area of the clot. In this case, for the quantitative analysis, the borderline between the inner and outer layers was drawn through the middle of the transition zone. It was not always possible to see the distinct packing zones in the clots with ~10% extent of contraction, so the quantitative data at the smallest extents of contraction have been considered inaccurate and were considered as a trend, but excluded from the statistical analysis shown in Figure 3.

Section S2. *Dynamic composition of intermediately compressed RBCs and fibrin in blood clots during contraction*

In SEM images, the dynamics of intermediately compressed RBCs in various clot parts was less certain than fully compressed polyhedrocytes, but followed a similar general trend, depending on the degree of compression. The slightly deformed mainly biconcave RBCs decreased with contraction abruptly in the center, then went down gradually in the intermediate part and dropped to a minimum in the outer layer only at the highest extent of contraction (Figure S7A). The number of more deformed intermediate mainly polyhedral RBCs did not depend strongly on the extent of contraction and the location in the clot (Figure S7B).

A quantitative analysis of fibrin content and distribution showed that with an increase in the extent of contraction, fibrin accumulated gradually at the peripheral part of the clot and reached a maximum in the outer layer at 60% extent of contraction (Figure S8). Accordingly, as the extent of contraction increased, the content of fibrin in the intermediate and central parts of the clot decreased progressively due to redistribution of fibrin towards the outer layer.

Section S3. *Comparative structural analysis of the contracted clots formed in citrated and non-anticoagulated blood samples*

To see if the presence of citrate and abnormal $[Ca^{2+}]$ in the blood could affect the structure and cellular composition of clots, we formed clots in parallel from the same blood samples without and with addition of citrate that were allowed to contract for up to 1 hour after clot formation. 1 U/ml thrombin and 2 mM $CaCl_2$ (both final concentrations) were added to the citrated blood but only 1 U/ml thrombin was added to the non-anticoagulated blood sample to eliminate the difference between the blood clotting and clot contraction kinetics that might affect the clot structure. At certain time points of contraction, the clots were fixed and subjected to histological examination. The comparative analysis presented in Figure S13 shows that in the blood clots formed in the absence and presence of citrate, the dynamic content of biconcave and polyhedral RBCs was almost the same. Therefore, the data on RBC deformation during clot contraction performed in the *in vitro* clots from citrated blood are adequate to represent the RBC compression in the *in vivo* thrombi formed in the absence of citrate.

Section S4. *The extents of intravital contraction of the atherothrombogenic and the cardioembolic cerebral arterial thrombi determined based on their cellular composition*

For the arterial cerebral thrombi, we analyzed the extent of intravital contraction in two subgroups of patients with atherothrombogenic (n=9) and cardioembolic (n=15) stroke. No significant difference was revealed; the average extents of contraction were 43±7% and 46±2% (p>0.05, Mann-Whitney test) for the atherothrombogenic and the cardioembolic stroke patients, respectively. As a matter of fact, the average age of thrombi (determined by the time from the stroke inception to thrombectomy) between the two subgroups of stroke patients was also indistinguishable and comprised 4±3 hours and 5±2 hours (p>0.05) for atherothrombogenic and the cardioembolic thrombi, respectively. Perhaps there was no significant difference because of the relatively small number of samples and/or high scatter.

Section S5. *Additional comparative analysis of the extents of intravital contraction of arterial and venous thrombi and thrombotic emboli determined based on their cellular composition*

In addition to the commonly used Mann-Whitney U test, the extent of contraction of arterial versus venous thrombi and their parts was performed using analysis of similarities (ANOSIM), although it is not commonly used in biomedical research. The ANOSIM is a non-parametric statistical ANOVA-like test that uses a matrix of rank dissimilarities to test whether it is possible to reject the null hypothesis that the similarity between groups is greater than the similarity within the groups. The R-statistic in ANOSIM is a ratio between within-group and between-group dissimilarities. We calculated ANOSIM (p<0.05) both between all groups and in pairs (with a correction for multiple comparisons). Both major parameters (the extents of contraction and biconcave/polyhedral RBCs ratios) were used. The ANOSIM test revealed a significant difference for only the tail of venous thrombi vs arterial thrombi (R=0.291, p=0.03). This result means that the samples within each of these groups (similar type of thrombi) are more similar to each other than when compared between these two groups (different types of thrombi). A more detailed test algorithm is described in the caption to Figure S14.

The results obtained with ANOSIM confirmed the conclusions drawn earlier on the basis of conventional statistical analysis performed using a non-parametric Mann-Whitney U test (Figure 7).

Supplemental Tables

Table S1. Content of the RBC types with various degrees of compression in blood clots (n=27) at different extents of clot contraction

Extent of clot contraction	Biconcave RBCs, %	Intermediate mainly biconcave RBCs, %	Intermediate mainly polyhedral RBCs, %	Polyhedral RBCs, %
10%	14 [7;29]	50 [9;66]	31 [5;82]	0 [0;0]
20%	4 [0;16]	17 [1;69]	57 [10;78]	0 [0;25]
30%	3 [0;14]	20 [0;44]	31 [47;79]	1 [0;20]
50%	0 [0;3]	1 [0;20]	79 [14;87]	3 [0;19]
60%	0 [0;1]	0 [0;0]	21 [1;73]	40 [7;99]

Median [interquartile range]

Table S2. Composition of the individual blood samples from patients with COVID-19 (n=23) used to train a "contraction ruler" with pathologically altered blood samples

Patient, #	Fibrinogen, g/l	Hematocrit, %	Platelets, $\times 10^9/l$
1	3.3	24	60
2	2.8	43.9	191
3	4.4	38.8	210
4	4.8	41	156
5	3.7	29.4	244
6	3.9	42.1	246
7	8.6	33.9	215
8	4.7	30.1	36.5
9	4.1	43	273
10	3.8	39	205
11	5.1	37.6	222
12	3.7	37.3	273
13	6.6	42.6	341
14	4.1	29	103
15	5.1	44.6	200
16	5.7	36.3	225
17	7.1	38.8	87
18	5.6	37	190
19	5.5	38.7	156
20	6.1	33	193
21	4.6	43	337
22	4.8	41	355
23	5.1	46	255

Table S3. Demographic and clinical characteristics of the COVID-19 patients enrolled in this study

Characteristics		Number of patients (n=23)
Sex, female		10 (43%)
Age, years	<65	8 (35%)
	≥65	15 (65%)
The severity of the disease	Moderate*	17 (74%)
	Severe*	6 (26%)
The extent of lung damage (CT scan)	Mild*	6 (26%)
	Moderate*	11 (48%)
	Severe*	6 (26%)
Duration of the disease at the time of examination	<7 days from onset of the disease	2 (9%)
	7-14 days from the onset of the disease	9 (39%)
	>14 days from onset of the disease	12 (52%)
Outcome of the disease	Favorable	21 (91%)
	Lethal	2 (9%)
Comorbidities and risk factors		
Neoplasms of hematopoietic or lymphoid tissues		2 (9%)
Hypertension		9 (39%)
Diabetes		5 (22%)
Coronary heart disease		4 (17%)
Acute myocardial infarction		3 (14%)
Cerebral ischemic stroke or transient cerebral ischemic attacks		6 (26%)
Phlebitis and thrombophlebitis of superficial vessels of lower extremities		1 (4%)
Smoking		3 (14%)
Obesity (BMI > 30 kg/m2)		10 (43%)
Therapy		
Low molecular weight heparin	Standard prophylactic dose (enoxaparin 0.5 mg/kg once daily)	17 (74%)
	High prophylactic and therapeutic doses (enoxaparin 0.5 or 1.0 mg/kg twice daily)	6 (26%)
Glucocorticosteroids (dexamethasone, methylprednisolone, prednisolone)		23 (100%)
Interleukin-6 inhibitors (tocilizumab)		2 (9%)
Antiviral drugs (ingavirin, arbidol)		4 (17%)
Mucolytics (ACC, ambroxol)		8 (35%)
Hydroxychloroquine		8 (35%)
Mechanical ventilation		1 (4%)

*Disease severity and the extent of lung damage were defined according to the temporary guidelines "Prevention, diagnosis and treatment of the new coronavirus infection (COVID-19)" issued on February 9, 2021, by the Ministry of Health of the Russian Federation.

Table S4. The extent of contraction of individual venous thrombi and their parts determined using the "contraction ruler"

Venous thrombi, ##	Ratio: polyhedral/biconcave RBCs	Extent of contraction, %
Head		
1	15	39
2	87	46
3	208	49
4	81	46
5	38	43
6	91	46
7	9	37
8	3	33
9	43	43
10	14	38
11	194	49
12	227	49
13	207	49
Body		
1	0	-
2	17	42
3	235	42
4	21	42
5	4	41
6	31	42
7	7	41
8	0	-
9	37	42
10	8	41
11	29	42
12	104	42
13	64	42
Tail		
1	4	34
2	4	34
3	38	43
4	0	-
5	0	-
6	0	-
7	7	36
8	0	-
9	4	34
10	1	-
11	15	39
12	62	44
13	41	43

Table S5. The extent of contraction of individual pulmonary emboli determined using the "contraction ruler"

Pulmonary emboli, ##	Ratio: polyhedral/biconcave RBCs	Extent of contraction, %
1	14	38
2	4	34
3	8	37
4	3	33
5	77	45
6	21	40

Table S6. The extent of contraction of individual arterial cerebral thrombi determined using the "contraction ruler"

Cerebral arterial thrombi, ##	Ratio: polyhedral/biconcave RBCs	Extent of contraction, %
1	27	41
2	89	45
3	56	44
4	107	46
5	34	42
6	319	50
7	225	50
8	10	38
9	145	48
10	267	50
11	459	52
12	48	44
13	202	49
14	564	52
15	674	53
16	59	44
17	111	46
18	2	32
19	35	42
20	564	52
21	4	33
22	4	33
23	226	49
24	40	43

Table S7. Composition of the blood samples from healthy subjects used to create a "contraction ruler"

Parameters	Mean ± SD (n=9)
Fibrinogen, g/l	3.5±0.1
RBCs, ×10^{12}/l	4.2±0.4
Hematocrit, %	38±4
Platelets, ×10^9/l	239±81
WBCs, ×10^9/l	4.6±0.3

Table S8. Demographic and clinical characteristics of patients with deep venous thrombosis enrolled in this study (n=13)

Clinical data		Patients, n (%)
Average age, years		62±6
Sex, female		7 (54%)
Prior history of DVT or PE		5 (38%)
Floating part of the thrombus	≥ 7 cm	3 (23%)
	< 7 cm	10 (77%)
Location of the thrombus	Proximal	8 (62%)
	Distal	5 (38%)
Duration of symptoms	≥ 21 days (subacute)	3 (23%)
	< 21 days (acute)	10 (77%)
Pulmonary embolism	No	6 (46%)
	Yes	7 (54%)
Use of anticoagulants and antiplatelet drugs	No	11 (85%)
	Yes	2 (15%)
Hemostatic and hematological parameters		
Parameters (normal ranges are shown in parentheses)		*Mean ± SD*
Fibrinogen (1.8–4.0), g/L		3.8 ± 0.4
Platelet count (180–320), $\times 10^9$/L		285 ± 14
Red blood cells (3–5), $\times 10^{12}$/L		4.1 ± 0.2
Hematocrit (36–48), %		37 ± 0.2

Table S9. Demographic and clinical characteristics of patients with pulmonary embolism enrolled in this study (n=6)

Clinical data		Patients, n (%)
Average age, years		64±11
Sex, female		3 (50%)
Prior history of DVT or PE		5 (83%)
Comorbidities	Hypertension	5 (83%)
	Diabetes	2 (33%)
Risk factors	Cancer	1 (17%)
	Postoperative state	3 (50%)
	Immobility or decreased mobility	4 (67%)
	Obesity	2 (33%)
Postmortem interval	< 24 hours	5 (83%)
	≥ 24 hours	1 (17%)
Cause of death	Directly due to PE/saddle embolus	3 (50%)
	PE contributed to multifactorial causes of death	3 (50%)
Location of PE	Saddle PE	3 (50%)
	Main pulmonary arteries or lobar pulmonary artery	2 (33%)
	Segmental and subsegmental pulmonary artery	1 (17%)
Use of anticoagulants and antiplatelet drugs	Yes	6 (100%)

Table S10. Clinical characteristics of patients with acute ischemic stroke enrolled in this study (n=24)

Clinical data		Patients, n (%)
Average age, y		72±7.9
Sex, female		11 (46%)
Etiology	Atherothrombogenic stroke	9 (38%)
	Cardioembolic stroke	15 (63%)
Stroke severity at the time of admission	NIHSS score, ≤10	1 (4%)
	NIHSS score, 11-20	16 (67%)
	NIHSS score, 21-30	7 (29%)
Stroke severity 24 h after admission	NIHSS score, ≤10	11 (46%)
	NIHSS score, 11-20	7 (29%)
	NIHSS score, 21-30	3 (13%)
Stroke severity 7 d admission	NIHSS score, ≤10	12 (50%)
	NIHSS score, 11-20	7 (29%)
	NIHSS score, 21-30	3 (13%)
Stroke outcome 3 mo after admission	mRS score, ≤2	5 (21%)
	mRS score, 3	6 (25%)
	mRS score, 4-5	7 (29%)
	mRS score, 6	6 (25%)
Thrombolysis	Yes (Actilyse)	15 (63%)
	No	9 (38%)
Thrombosis duration	≥240 min	7 (29%)
	<240 min	15 (63%)
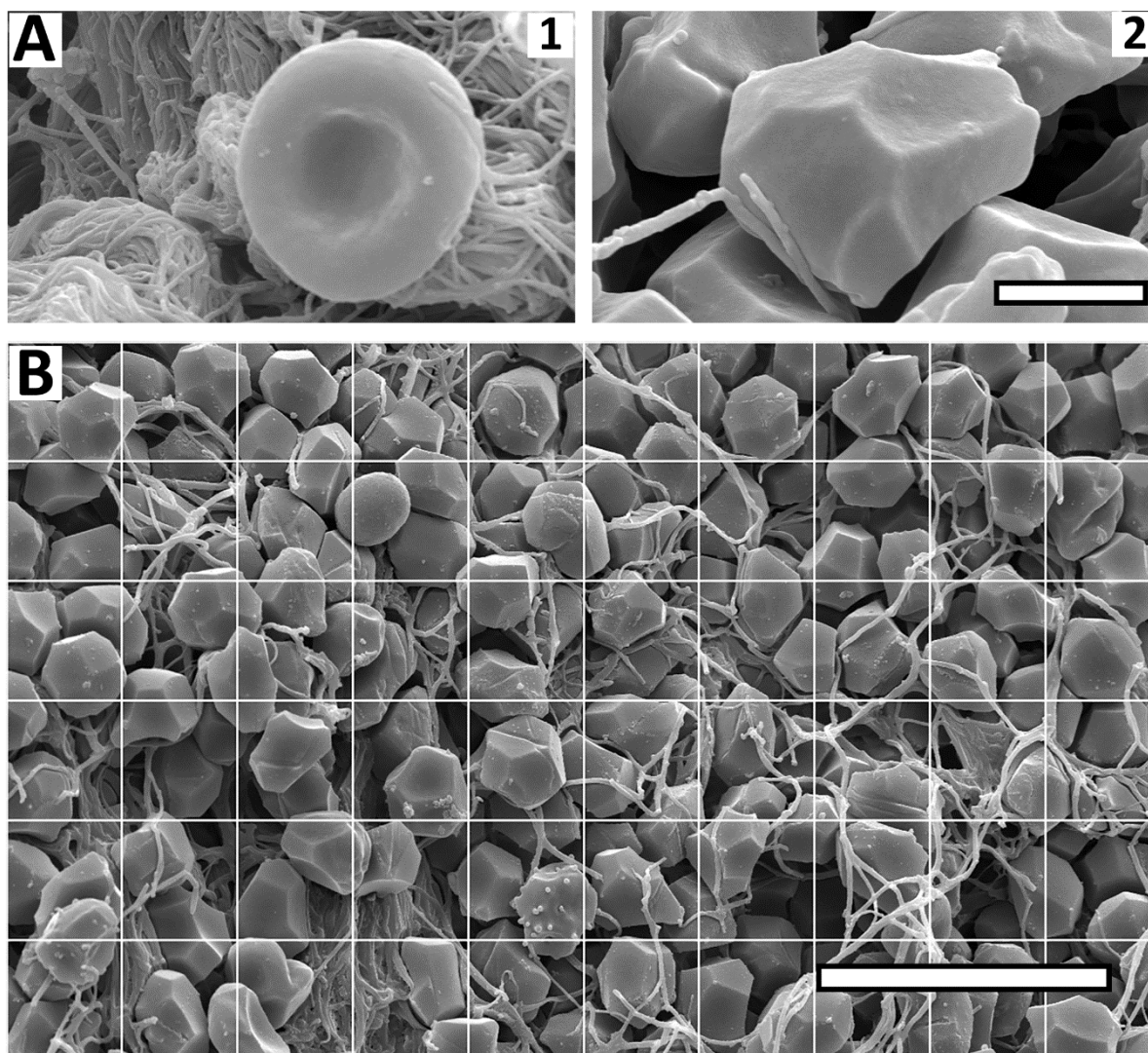
Figure S1. Imaging and quantification of the structural elements of *ex vivo* thrombi using high-resolution scanning electron microscopy. (**A**) Selected portions of scanning electron micrographs of thrombi, illustrating the structures analyzed in this study: a biconcave RBC (*1*), a polyhedral compressed RBC (polyhedrocyte) (*2*). Magnification bar = 3 μm. (**B**) A scanning electron micrograph with overlaid grid (the size of each square is 6 μm x 6 μm) used to quantify the cellular composition of a thrombus. Each grid square contains several cells that were marked and measured. The number for each RBC type per image was counted. The total area of each image taken at a 2,000× magnification was 36 μm × 60 μm = 2,160 μm^2. Magnification bar = 15 μm.
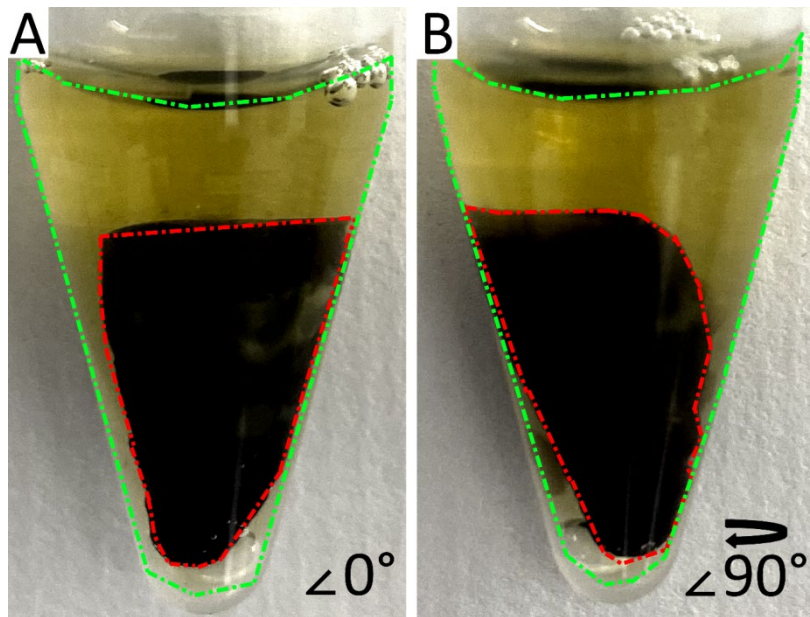
Figure S2. Perpendicular photographic images of the same contracted *in vitro* clot made in 1.2 ml citrated blood (final 2 mM $CaCl_2$, 1 U/ml thrombin, 37°C, 60 min). To determine the extent of clot contraction, the areas corresponding to the initial clot volume (within *green dashed line*) and the volume of contracted clot (within *red dashed line*) were measured using ImageJ software. In the example presented, the area of the contracted clot comprises 48% of the initial area in **A** and 49% in **B**. The ultimate extent of contraction was determined as an average between the perpendicular photographs.
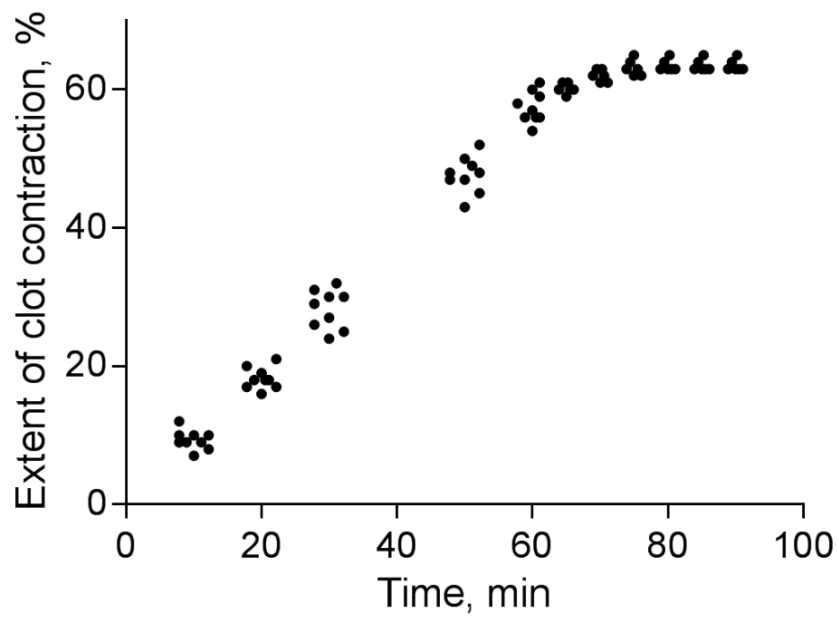
Figure S3. The extent of clot contraction as a function of time for clots formed from the blood of healthy donors (n=9). After 60 min, the extent of contraction deviated from the linearity and plateaued at 80-90 minutes.
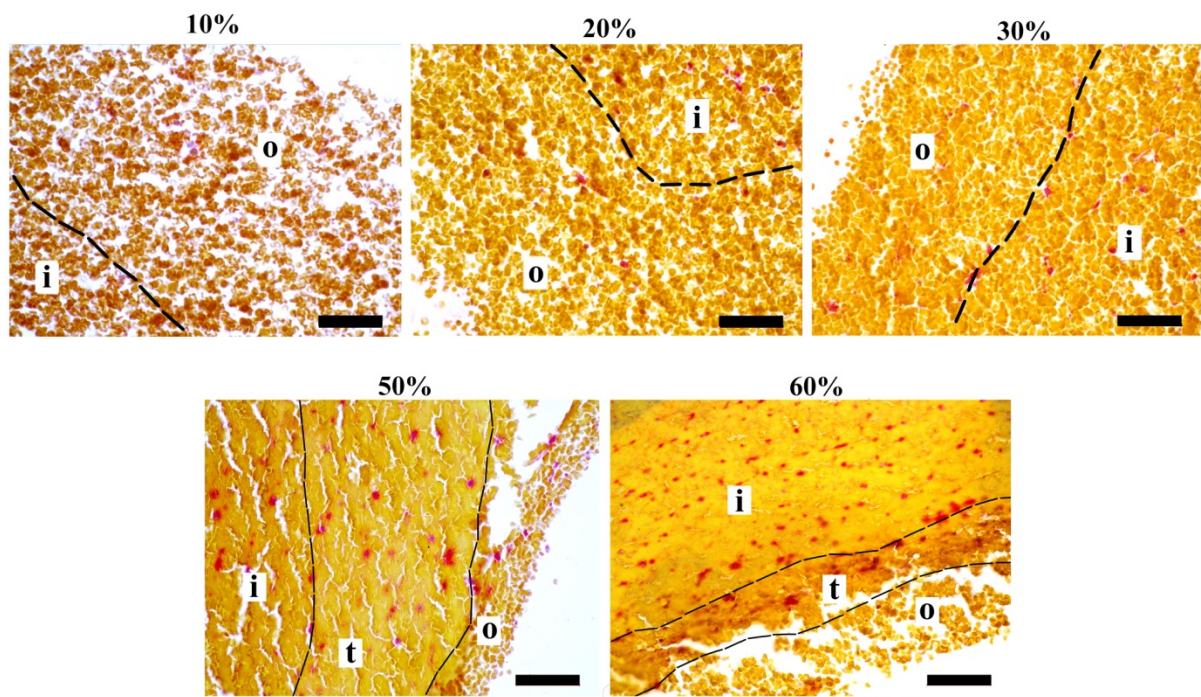
Figure S4. Representative histological images of blood clots with various extents of contraction. Picro-Mallory stain. 400×, magnification bars = 50 µm. Designations: "*o*" – outer layer and *"i"* – inner portion separated by a dashed line. Layers could be distinguished by the packing density of erythrocytes. Sometimes a transitions area with an intermediate packing density was observed (designated *"t"* at the 50% and 60% extents of contraction).
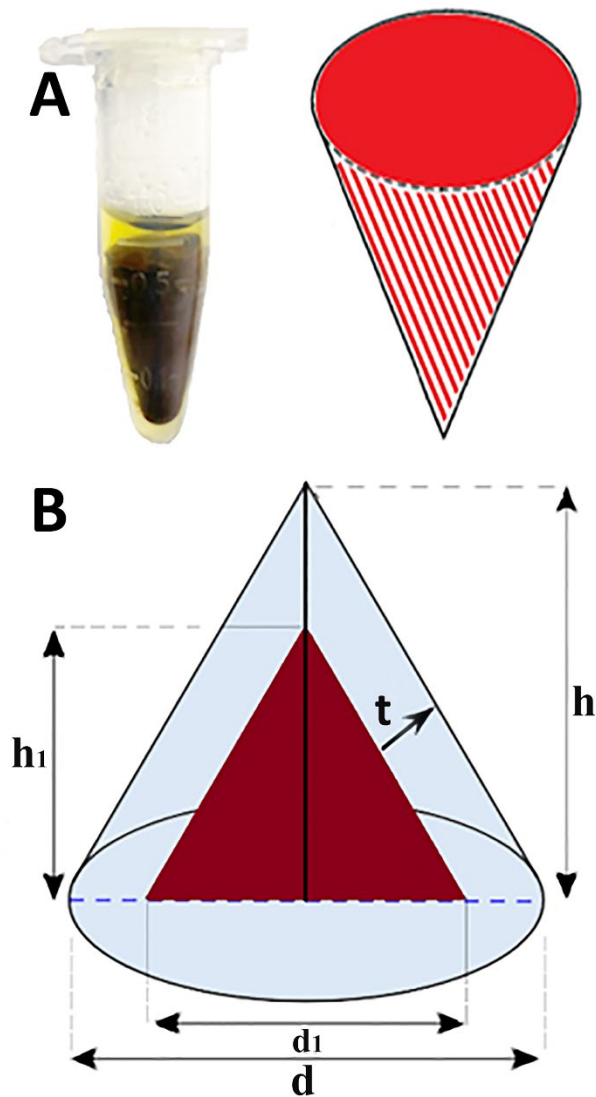
Figure S5. A macroscopic image of an *in vitro* blood clot and a schematic diagram showing clot portions discerned and measured microscopically. (**A**) Overall geometry of a contracted blood clot represented roughly as a cone. (**B**) Schematic diagram of a conical contracted blood clot after middle longitudinal sectioning. The following parameters were used to calculate the volume fractions of the outer layer and inner portion: d – total cone diameter, d_1 - diameter of the inner portion, h – total cone height, h_1 - height of the inner portion, t – thickness of the outer layer. The dimensions and the volume of the outer layer were measured and calculated directly from the histological preparations, and the volume of the inner portion was determined by subtracting the volume of the outer layer from the entire volume of the clot.
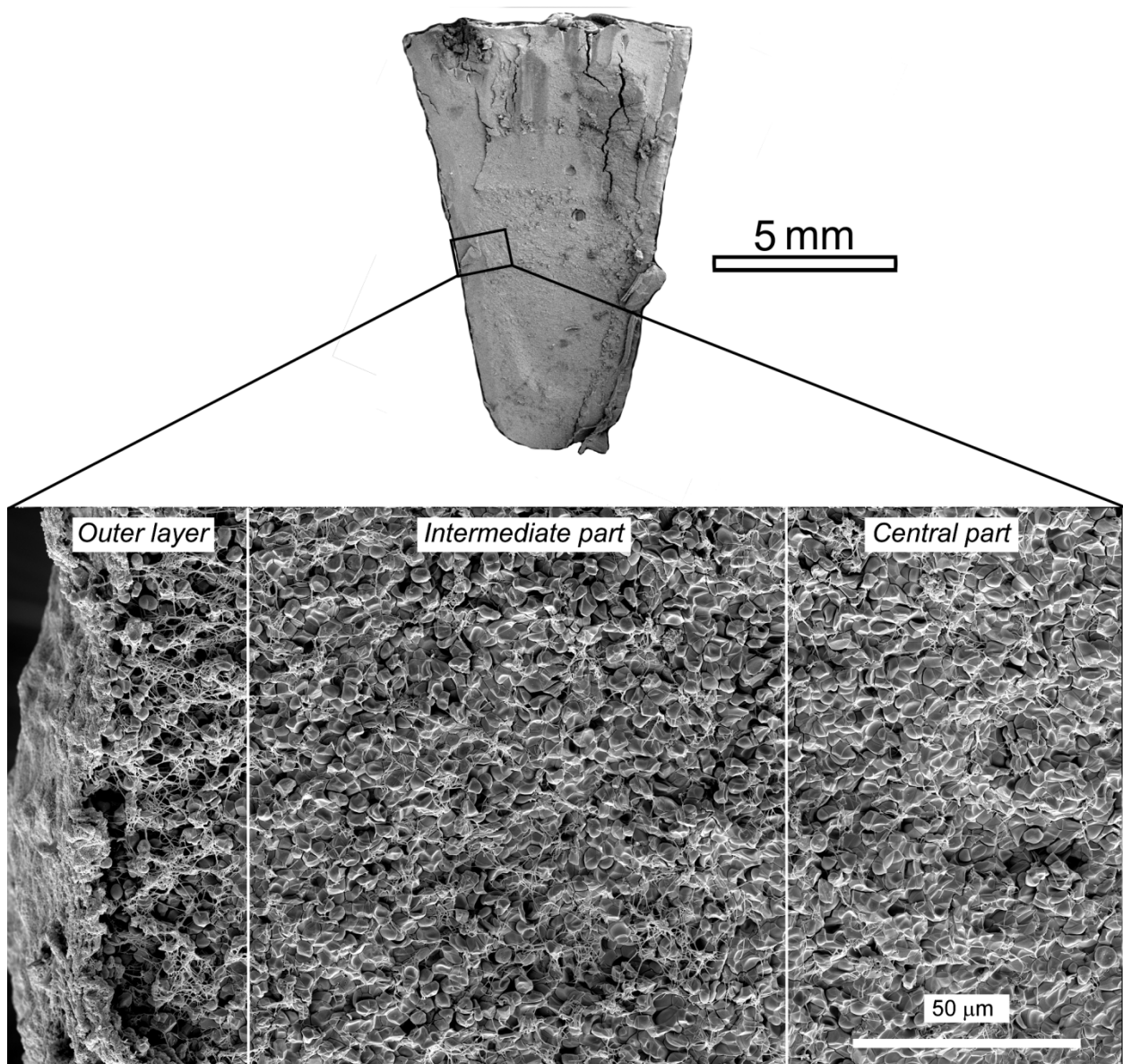
Figure S6. Zoomed in (not to scale) panoramic scanning electron micrograph (technology of our scanning electron microscope to stitch together hundreds of adjacent images) of a contracted blood clot showing: 1) superficial fibrin-platelet agglomeration, fibrin network, and sparse non-deformed RBCs in the outer layer, 2) a mixture of fully and partially deformed RBCs with some intercellular spaces and fibrin fibers in the intermediate part and 3) tightly packed tessellated polyhedrocytes without spaces and no fibrin in the central part of the clot.
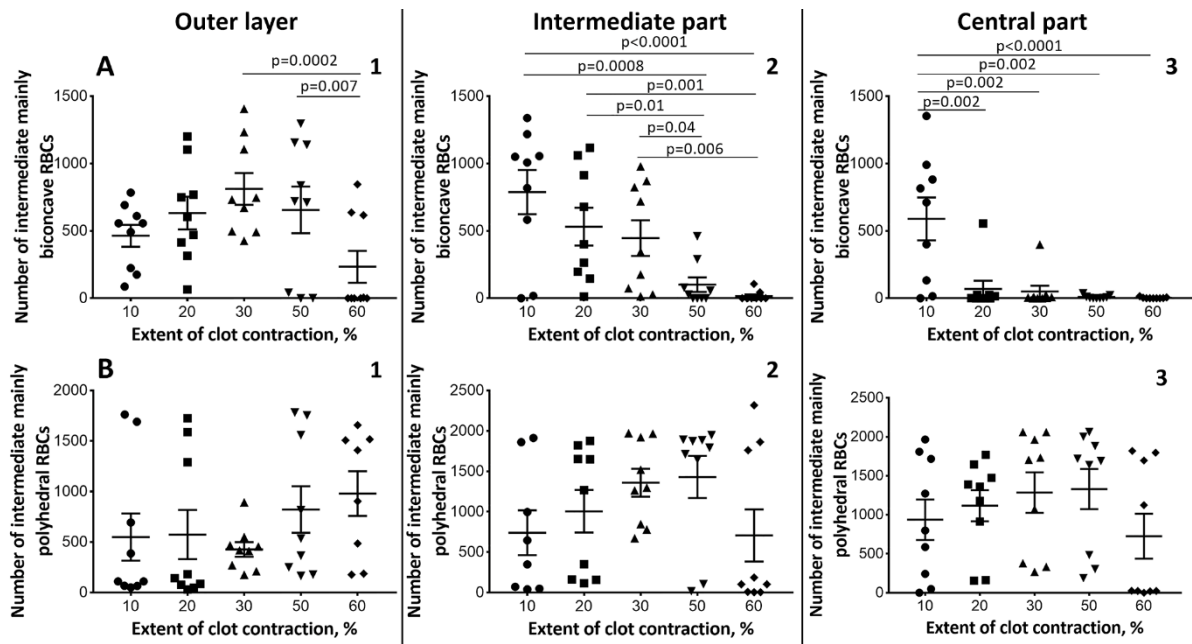
Figure S7. Dot-plots showing the absolute number of intermediate mainly biconcave RBCs (A) and intermediate mainly polyhedral RBCs (B) in the clots from normal blood samples with different extents of contraction. A number of RBCs was calculated per image area in the periphery (*1*), intermediate part (*2*) and center (*3*) of a clot. Each dot (n=9) represents a number of cells of a certain type calculated from 1 of 3 individual scanning electron micrographs, each covering a certain area (~36,700 μm²), from 9 individual blood clots. Results are presented as the median with interquartile range. Statistical analysis: (A) nonparametric Friedman test with post hoc Benjamini, Krieger and Yekutieli test; (B) Kruskal–Wallis test with Dunn's post hoc test (*1*, *2*), Friedman test with post hoc Benjamini, Krieger and Yekutieli test (*3*).
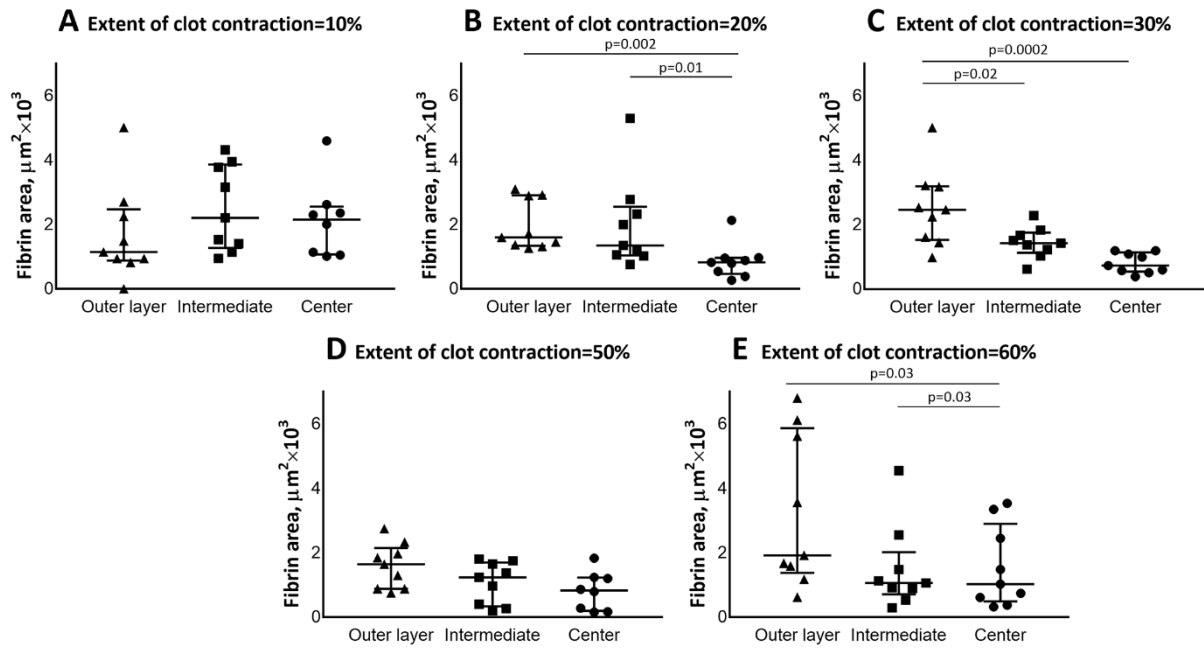
Figure S8. Dot-plots showing the amount of fibrin in the outer layer, intermediate part and center of blood clots with different extents of contraction (A-E). Each dot represents a fibrin-occupied area from individual scanning electron microscopy images of 9 individual blood clots. Fibrin is accumulated at the clot outer layer with an increasing extent of contraction. Results are presented as the median with interquartile range. Statistical analysis: one-way ANOVA (A, C, D) and Friedman test (B, E) with post hoc Holm-Sidak and Benjamini, Krieger and Yekutieli multiple comparisons tests. In A and D there was no significant difference between the variances ($p>0.05$).
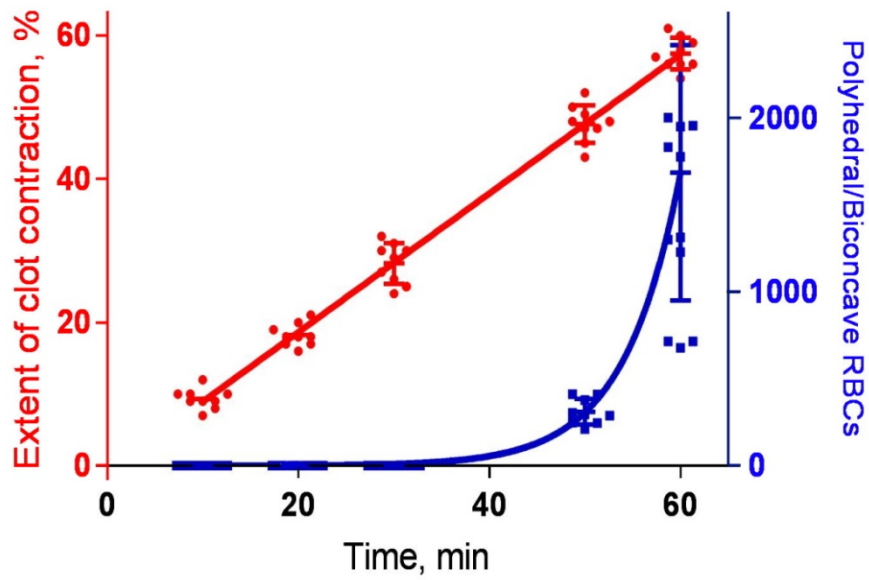
Figure S9. The extent of clot contraction (red line) and the polyhedral/biconcave RBCs ratio (blue line) as a function of time in the clots formed from the blood of healthy donors (n=9). The extent of clot contraction is fitted to a linear function ($R^2=0.96$), while the polyhedral/biconcave RBCs ratio is fitted to the exponential ($R^2=0.83$). The results are presented as a median with error bars comprising 95% CI.
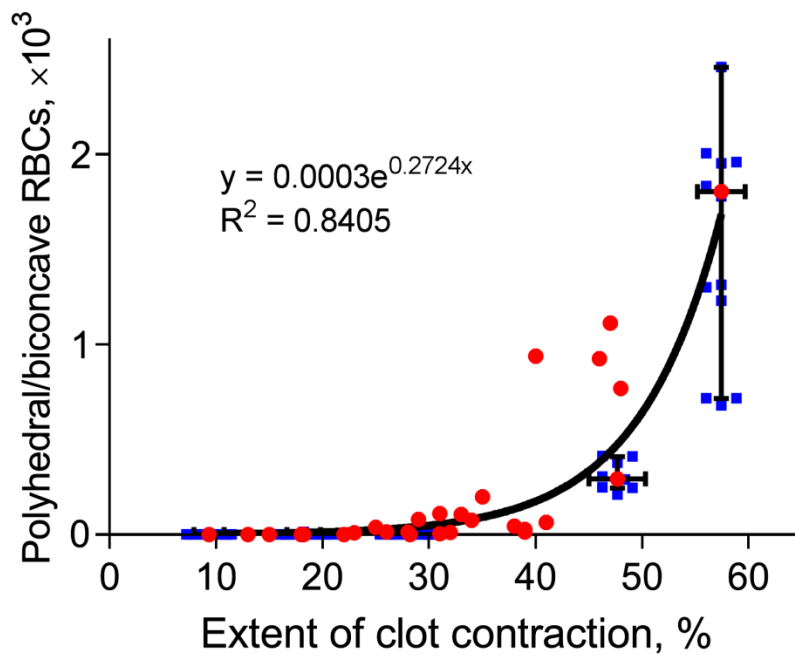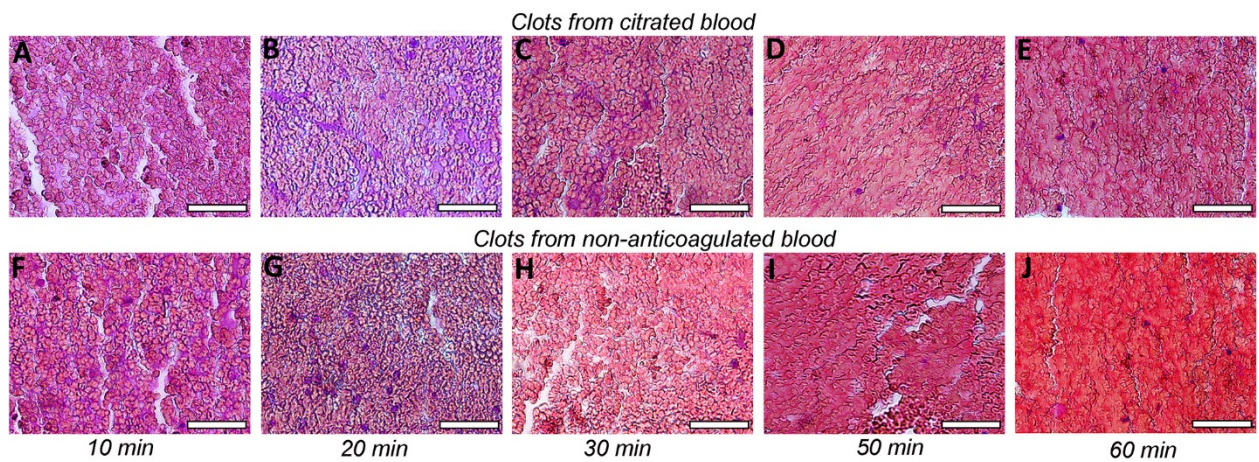
Figure S10. The polyhedral/biconcave RBC ratio as a function of the extent of clot contraction fitted with an exponential (R^2=0.84) for <u>clots formed from normal (blue squares) and pathological (red dots) blood samples</u>. This plot is described by a mathematical function: y=0.0003*exp(0.2724x).The results are presented as a median with error bars comprising 95% CI.
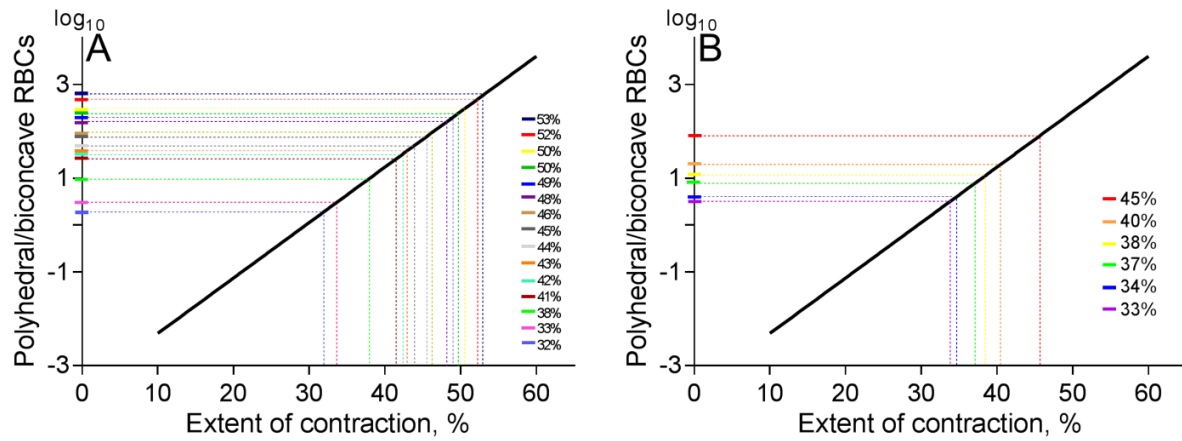
Figure S11. The "contraction ruler" used to assess the extent of intravital contraction for individual cerebral thrombi (A) and pulmonary emboli (B) based on their cellular composition. The polyhedral/biconcave RBC ratio (Y-axis) determined for a thrombus from a set of scanning electron micrographs is extrapolated to the X-axis to determine the corresponding extent of contraction. The "ruler" is based on the precise quantification of the cellular composition of *in vitro* blood clots with various known extents of contraction (see Figure 5).
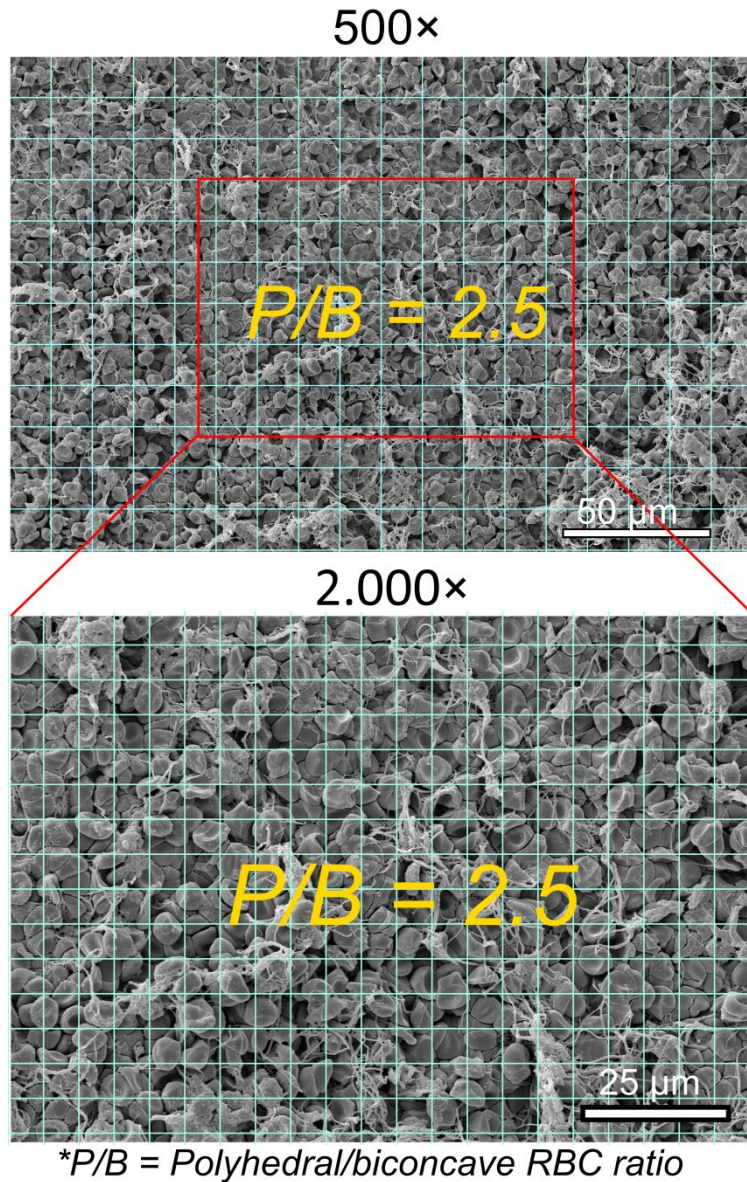
Figure S12. Two images of the same clot at 500× and 2,000× normalized by the area covered along with the polyhedral/biconcave RBC ratios obtained for each image. The upper and lower images represent the same area, but the size of the grid squares is different (14 µm×14 µm and 6 µm×6 µm, respectively), which does not affect quantifications of the cellular composition.

Clots from citrated blood

Clots from non-anticoagulated blood

10 min   20 min   30 min   50 min   60 min

Figure S13. Microscopic representation of the dynamic shape change and packing density of RBCs in clots formed from normal citrated blood (**A–E**) and from the same blood without an anticoagulant (**F–J**) at different time points after formation and contraction (up to 60 min). Both in the presence (*upper row*) and absence (*lower row*) of citrate, biconcave RBCs gradually undergo densification and the compressive deformation from biconcave to polyhedral shape. Hematoxylin and eosin, 400×, magnification bars = 50 μm.
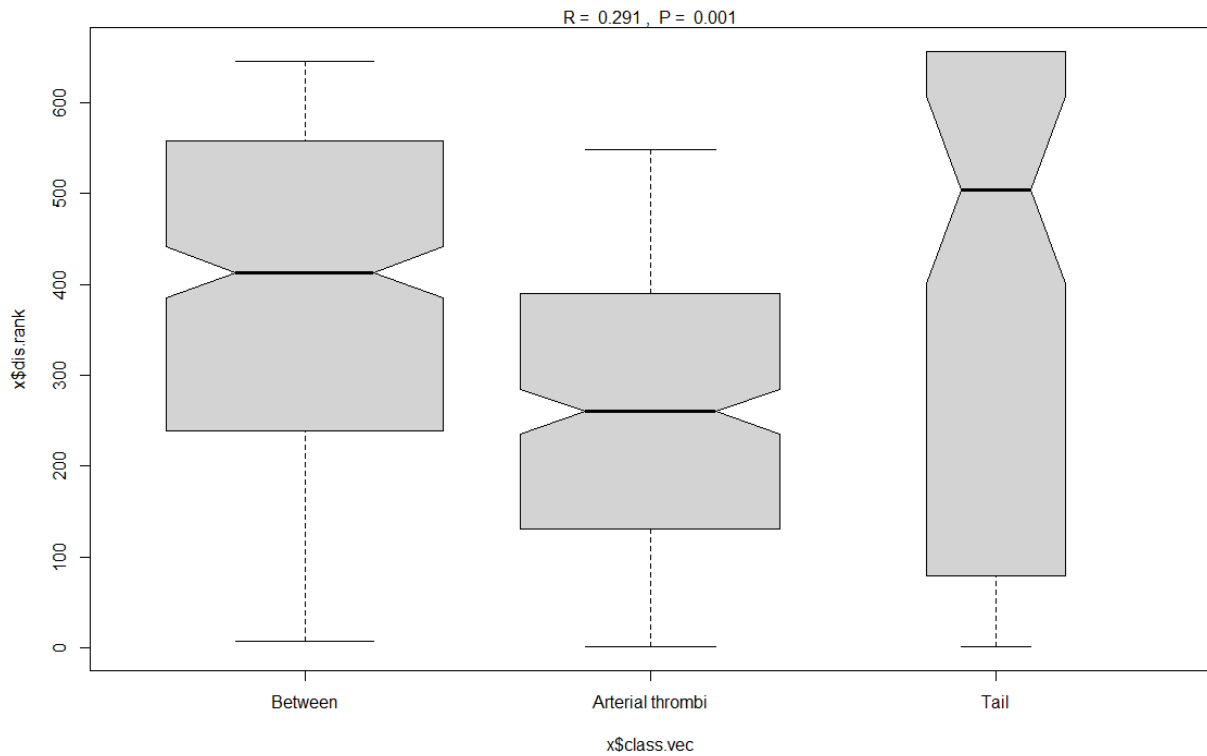
Figure S14. **The ANOSIM test for the tails of venous thrombi vs. arterial thrombi (R=0.291, p=0.03).** The analysis was done in the following steps: 1) calculate a matrix of dissimilarity scores for every pair of sites; 2) convert the dissimilarities to ranks; 3) calculate the R statistic as the ratio between dissimilarities between sites within a group and the dissimilarities between sites that are in different groups - the closer this value is to 1, the more the sites within a group are similar to each other and dissimilar to sites in other groups; 4) the significance of the R-statistic is determined by permuting the membership of sites in groups.